J Appl Electrochem (2011) 41:669–679
DOI 10.1007/s10800-011-0279-y

ORIGINAL PAPER

Effect of aromatic aldehydes on the electrodeposition of ZnCo alloy from cyanide-free alkaline-gluconate electrolytes

José Luis Ortiz-Aparicio · Yunny Meas · Gabriel Trejo · Raúl Ortega · Thomas W. Chapman · Eric Chainet · Patrick Ozil

Received: 18 November 2010 / Accepted: 3 March 2011 / Published online: 17 March 2011

Abstract The effects of vanillin and anisaldehyde on electrodeposition of zinc–cobalt alloys onto AISI 1018 carbon steel were studied in an alkaline gluconate zincate electrolyte. The influence of an additive on the metal discharge depends on the structure of the added molecule and on the nature of the substrate. The composition of the deposit varies during the electrodeposition process. Maximum cobalt content is observed close to the steel–ZnCo interface for ZnCo formed with or without vanillin, but the composition profile becomes more uniform when anisaldehyde is added to the bath. The morphology of Zn-rich Co-alloy coatings was evaluated: Cobalt ions produce porous ZnCo alloys; vanillin induces slightly porous deposits, whereas uniform and more compact deposits were observed with anisaldehyde. Furthermore, a crystallographic study showed that the orientation of the lattice planes changes, with highly oriented deposits produced in the presence of anisaldehyde.

J. L. Ortiz-Aparicio · Y. Meas (✉) · G. Trejo · R. Ortega · T. W. Chapman
Centro de Investigación y Desarrollo Tecnológico en Electroquímica, Parque Tecnológico Querétaro, Sanfandila, 76703 Pedro Escobedo, Querétaro, Mexico
e-mail: yunnymeas@cideteq.mx

Present Address:
J. L. Ortiz-Aparicio
Centro Nacional de Metrología, Carretera a los Cués, Km 4,5, 75246 El Marques, Querétaro, Mexico

E. Chainet · P. Ozil
Laboratoire d′Electrochimie et Physico-Chimie des Matériaux et Interfaces, UMR 5631 CNRS-Grenoble INP-UJF, PHELMA, BP75, 38402 Saint Martin d′Hères, France

Keywords Zinc · Cobalt · Alloy electrodeposition · Aromatic aldehydes · Organic Additives

1 Introduction

ZnCo alloys are important due to improved corrosion resistance of steel substrates compared with pure Zn coatings [1–3]. Zinc codeposition with metals of the iron group favors the preferential deposition of the less noble metal (zinc); this phenomenon has been described as anomalous codeposition by Brenner [4]. Various electrolytes have been proposed for ZnCo-alloy electrodeposition using slightly acidic [5] or moderately [6] or highly alkaline baths [7, 8]. These latter formulations have been developed especially to avoid cyanide-based baths [1–3]. Their formulations often include small amounts of organic compounds as additives [1]. These compounds are important in the composition of alkaline baths for Zn and Zn–iron-group alloy deposition because they modify the crystal growth and therefore change the mechanical properties and appearance of the coatings [1–3].

The effects of several organic compounds on zinc electrodeposition have been investigated previously [9–13]. Clear effects of the additives are observed, such as decreasing the grain size, increasing the overpotential of zinc reduction, and improving the appearance of the product, among others [1–3]. These effects are often attributed to the blocking of active sites by adsorption of organic molecules that to form a barrier on the surface. The influence of triethanolamine and gelatin on the electroplating parameters during the deposition of ZnCo alloys from an alkaline bath was studied [14, 15]. Quaternary ammonium compounds (QACs) have been used as brightening additives in alkaline zinc electrolytes [16–19].

A study was recently performed to analyze the effects of the chemical structure of a family of QACs on ZnCo deposition [7]. It was found that QACs reduce significantly the grain size and change the crystallographic orientation of the deposits. Macromolecules have also been reported [20–23] because they lead to smooth and fine-grained deposits.

Although vanillin and anisaldehyde have been used extensively as additives in alkaline zinc-plating formulations [1, 11, 12], little research has been done. In an acidic bath, Park et al. [24] showed that o-vanillin is strongly adsorbed on an iron substrate affecting the underpotential deposition (upd) of zinc. Its presence has a leveling effect on zinc morphology. Identification of the products formed by the cathodic reaction of *p*-vanillin during zinc electrodeposition from alkaline electrolytes was performed previously [25], and the concerned authors reported that 2-methoxi-*p*-cresol seems to be the main product. Others characterized the diverse products of *p*-vanillin decomposition in strongly alkaline and neutral electrolytes [26]; they found that the main products are hydrovanilloin and vanillin alcohol in the respective cases.

Mirkova et al. [18] studied the influence of anisaldehyde bisulfite, *N*-benzylpyridinium-3-carboxylate, and a mixture of the two (without an exact indication of its composition) on Zn electrodeposition. In the presence of each of these additives, the deposition potential of Zn shifts slightly toward more negative potentials. The Zn-reduction process was found to be controlled by mass transport in the absence of additives, whereas the process is under kinetic control in the presence of anisaldehyde or the additive mixture. The kinetic limitation was less dominant with *N*-benzyl-3-carboxylpyridinium. In a further study, Monev et al. [19] investigated the influence of anisaldehyde bisulphite and *N*-benzylpyridinium-3-carboxylate on Zn electrodeposition. Both additives enhance the rate of the hydrogen-evolution process (HER), and additionally *N*-benzylpyridinium-3-carboxylate promotes substrate hydrogenation. Kavitha et al. [27] studied the effects of several carbonyl compounds and some of their products from condensation reactions with thiosemicarbazide. These additives can be used in either acidic or alkaline electrolytes, and the condensation product between furfuraldehydes and thiosemicarbazide provided the best results.

The aim of this study is to study the influence of two important organic additives (vanillin and anisaldehyde) on the parameters of ZnCo alloy electrodeposition from an alkaline-gluconate–zincate solution prepared with metal chlorides and sodium gluconate and to characterize the composition as well as the morphological and crystallographic properties of the coatings formed on steel. These organic additives were chosen because of their similarities in molecular size, electronic density, and chemical structure, which involve aromatic aldehydes and methoxy groups.

2 Experimental

Electrodeposition studies were carried out from alkaline solutions of 0.25 M $ZnCl_2$ (Merck) mixed with sodium gluconate, and sodium hydroxide in aqueous solution with 5% ethanol to enhance the low solubility of the organic additives used in this study. All the solutions were prepared with deionized water (18 MΩcm). The Zn and Co coatings were deposited on an AISI 1018 carbon steel substrate. The stock plating-solution formulations are presented in Table 1, where L^- represents the gluconate anion. The organic additives *p*-vanillin (4-hydroxy-3methoxy-benzaldehyde, Fluka) and *p*-anisaldehyde (4-methoxy-benzaldehyde, Aldrich) were of analytic grade. The additives were dissolved in an ethanol stock solution before being added to the electrolyte.

The electrochemical experiments were performed with an Autolab Potentiostat/Galvanostat (PGSTAT 30). Cyclic voltammetry was carried out in a typical three-electrode cell. The working electrode was AISI 1018 steel embedded in a Teflon (PTFE) rod and offered a geometrical area of 0.032 cm^2. The reference electrode was a saturated calomel electrode (SCE), and the counter electrode was a graphite bar. The experiments were carried out under an atmosphere of ultrapure nitrogen. Before each experiment, the steel electrode was polished with 0.05 μm alumina (Buehler) to give a mirror-surface appearance. The solution was used at ambient temperature. Thin films were obtained potentiostatically from the plating solutions (Table 1) on the steel disk electrodes. The morphology of ZnCo deposits was examined by scanning electronic microscopy (JEOL DSM-5400 LV). X-rays diffraction experiments were performed in a Brucker X-ray diffractometer (D8 Advance) using CuKα radiation. Elemental analysis was performed in a Leco Glow Discharge Spectrometer (GDS) (Model 850A).

Table 1 Base composition of electrolytes for Zn, Co, and ZnCo electrodeposition
L^- gluconate anion

Solution	Composition
S_0	0.25 M $ZnCl_2$ + 4 M NaOH + 0.15 M NaL + 5% EtOH
S_1	0.01 M $CoCl_2$ + 4 M NaOH + 0.15 M NaL + 5% EtOH
S_2	0.25 M $ZnCl_2$ + 0.01 M $CoCl_2$ + 4 M NaOH + 0.15 M NaL + 5% EtOH

3 Results and discussion

3.1 Electrochemical study

3.1.1 Electrodeposition of Zn, Co, and ZnCo without additives

Line a in Fig. 1 represents the cyclic voltammograms for Zn(II) solution S_0, a complexing gluconate electrolyte without other organic additives. Previous studies have shown that the dominant Zn(II) species in alkaline-gluconate electrolytes is the hydroxy-complex $Zn(OH)_4^{2-}$ [28, 29]. From previous studies [7, 8], it was observed that the hydrogen evolution reaction (HER) on steel substrates from alkaline Zn(II) solutions is highly suppressed; the reduction potential of HER shifts to more negative values. According to some authors [30, 31], the underpotential deposition (upd) of Zn inhibits the HER kinetics as the exchange current densities are very sensitive to the nature of the surface for this reaction. HER occurs slowly on Zn, whereas a larger exchange current density is observed on Co, Ni, and Fe [30]. A previous study has reported that the inhibition of HER in the presence of zinc ions in an alkaline bath results from the formation of a sub-monolayer of Zn on a ferrous substrate [30], therefore, it is assumed that the suppression of the HER in these experimental conditions is due to the Zn upd. A single reduction peak Ic is observed at $E_p(\mathrm{Ic}) = -1.587$ V vs SCE, corresponding to the reduction of the $Zn(OH)_4^{2-}$ species to Zn metal [7, 8, 28, 29]. Upon inverting the potential scan direction, a single oxidation peak Ia appears because of the electro-oxidation of the coating that formed during the cathodic scan. A predominance diagram computed in a previous study [7] showed that no gluconate–zinc complexes are formed under the experimental conditions of this study.

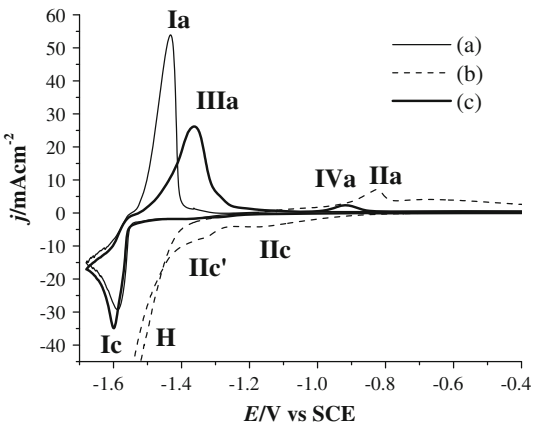

Fig. 1 Cyclic voltammograms recorded for: (**a**) solution S_0, (**b**) solution S_1, (**c**) solution S_2. v = 20 mV s^{-1} (See electrolyte compositions in Table 1)

The voltammogram of the S_1 electrolyte containing only cobalt ions with gluconate presents a cathodic wave around −1.2 V vs SCE (signal IIc in Fig. 1) and a second peak at −1.35 V (signal IIc′). This electrolyte is estimated to contain two gluconate complexes of Co(II) as 89.5% cobalt–hydroxo-gluconate species, $CoL_3(OH)_2^{3-}$ and 10.5% $CoL(OH)_2^-$ [7]. Under the working solutions, there is no formation of insoluble $Co(OH)_2$. Thus, $CoL_3(OH)_2^{3-}$ and $CoL(OH)_2^-$ may be considered as the electroactive species for Co(II) reduction, producing the two observed peaks. With a further increase in the cathodic current density, wave H appears and is due to the bulk HER, a concomitant process in metal electrodeposition [32] that is catalyzed by the cobalt deposit [7, 8, 30]. Upon reversing the potential scan, anodic peak IIa appears at −0.80 V vs SCE and is attributed to the stripping of pure cobalt that takes place simultaneously with the desorption of adsorbed hydrogen.

The addition of cobalt to the Zn(II) electrolyte (Solution S_2) modifies the cyclic voltammogram: the Zn cathodic peak potential (peak Ic) shifts to slightly more negative potentials in trace c ($E_p(\mathrm{Ic}) = -1.60$ V vs SCE). It is interesting to note that, when the scan is reversed to positive potentials, the oxidation peaks that appear are modified because of different alloys being formed during the cathodic scan. New oxidation peaks (IIIa and IVa) appear because of compositional changes of the deposit corresponding to the formation of different phases of ZnCo [33] during the cathodic scan. Such peaks associated with ZnCo phases are well known with acidic electrolytes [34–37]. Peak IVa appears around −0.9 V at a value more negative than the peak observed with the pure Co electrolyte and is attributed to a cobalt-rich alloy phase.

3.1.2 Effect of additives on ZnCo electrodeposition

In order to observe the effects of the aromatic aldehydes on alkaline-gluconate ZnCo electrodeposition, the cyclic voltammetry study was applied. Figure 2 presents the influence of vanillin and anisaldehyde on the electrochemical behavior during ZnCo deposition. Figure 2 (line a) shows a typical cyclic voltammograms for solution S_2.

When 5 mM vanillin is added to the bath, the reduction peak Ic is observed with a peak current density similar to that obtained without organic additives, thus indicating little effect of the additive on the electrodeposition process. A small signal IIc can be observed before peak Ic in Fig. 2, line b, corresponding to the deposition of cobalt or a cobalt-rich alloy. The massive reduction peak Ic appears at $E_p(\mathrm{Ic}) = -1.602$ V. At more negative potentials, around −1.75 V vs SCE, a crossover by the reverse scan is observed, suggesting a catalytic step. This may be caused by intermediates formed on the electrode during the electrochemical reduction of

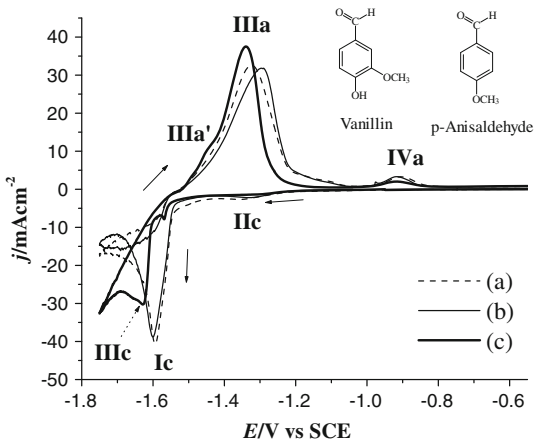

Fig. 2 Cyclic voltammograms for: (**a**) solution S_2, (**b**) S_2 + 5 mM vanillin, (**c**) S_2 + 5 mM anisaldehyde. v = 20 mV s^{-1}. S_2: 0.25 M $ZnCl_2$ + 0.01 M $CoCl_2$ + 4 M NaOH + 0.15 M NaL (see Table 1)

vanillin [25, 26] that could promote the HER. As the potential is scanned to positive values, the oxidation peaks appear, and peak IVa is still observed.

On the other hand, the reduction behavior is clearly modified more by incorporating anisaldehyde in the bath (Fig. 2, line c). The small peak IIc is decreased by the additive, which partially inhibits the Co(II) reduction [38]. A very small peak Ic is seen, but a second reduction peak IIIc appears at a more cathodic potential. This inhibition is characteristic of many organic additives and suggests the effect of adsorbed molecules that cover a portion of the active surface, thus requiring a greater potential to allow the metal discharge at peak IIIc [38]. According to these results, anisaldehyde increases the overpotential of ZnCo deposition more than vanillin does. When the potential scan was inverted to the positive direction, oxidation signals IIIa′ and IIIa were observed, the latter appearing at a more negative potential than that without the additive. Such changes may be related to changes in the composition of the Zn–Co alloys [34–37]. The additives could be playing a direct role in the electrochemical alloy-deposition reactions because the organic intermediates of carbonyl-based compounds formed on the electrode are known in some cases to participate in the Zn electrodeposition process [37–39].

3.1.3 *Effect of the switching potential, E_λ*

It is known that the composition of ZnCo alloys depends on the applied potential [5, 7, 8, 35–37]. Composition changes are indicated by the appearance of stripping peaks between the oxidation peaks of pure Zn and pure Co deposits. Therefore, the effect of the switching potential, E_λ, was studied with ZnCo deposits obtained from solution S_2 without and with additives to observe the variety of phases formed.

Figure 3 presents the cyclic voltammograms obtained when switching the potential scan at different cathodic

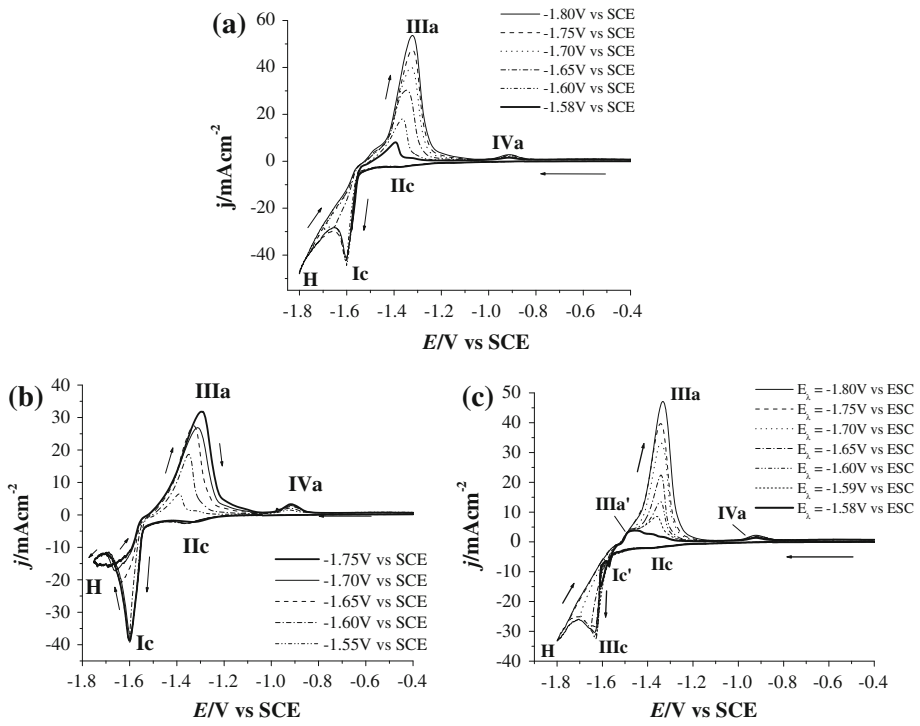

Fig. 3 Effects of varying the E_λ value on cyclic voltammograms recorded in solution. v = 20 mV s^{-1}. (**a**) S_2 without additives, (**b**) S_2 + 5 mM vanillin, (**c**) S_2 + 5 mM anisaldehyde

values. In Fig. 3a, the cathodic scan shows two reduction processes: the massive deposition of ZnCo leading to peak Ic, and a second cathodic process attributed to HER at more negative potentials (signal H). A gradual increase in the oxidation peak IIIa current occurs as E_λ is made more negative. The observed change of the stripping peaks with increasing polarization potential, E_λ, and in particular the split of the stripping peak IIIa at low E_λ values, indicate the occurrence of surface and bulk deposit transformations. The variation of the amount of metals deposited would increase the stripping charge, overlapping the signals due to the phases present in a minor content. Peak IVa also increases as E_λ reaches more negative values, which would be attributed to the formation of a cobalt-rich deposit. A small cathodic signal IIc appears at −1.35 V vs SCE. The variation of inversion potentials allows attribution of this peak to a cobalt-rich deposit since peak IVa appears only when the scan sweep is inverted after peak IIc; before peak IIc no stripping peak is observed. Thus, some cobalt electrodeposition seems to occur at low applied potentials. As the potential increases, massive ZnCo deposits form, the composition of the deposit changes, and anomalous deposits are formed, as can be inferred from the stripping signals.

In the presence of vanillin (Fig. 3b), the cathodic zinc peak Ic is inhibited slightly. When the voltammogram was scanned to more negative potentials ($E_\lambda = -1.75$ V), the cathodic signal close to the region of the HER increased, which may be due to a catalytic effect of the additive since the current increases with further additions of vanillin (not shown here). Alternatively, the current in this range may be due to a reaction of the additive. According to previous studies, vanillin is electroactive, and some electro-reduction products have been identified [25, 26]. This could explain the crossover seen at −1.7 V vs SCE. Stripping peaks IIIa and IVa still appear under these deposition conditions. Peak IIc is also observed, being associated with the deposition and stripping of a cobalt-rich phase (IVa).

Figure 3c shows that the addition of anisaldehyde changes the stripping profile. The voltammograms are different from those observed in Fig. 3a and b, thus indicating that anisaldehyde has a different effect on ZnCo reduction. In Fig. 3c the cathodic peak Ic vanishes, and massive ZnCo deposition (peak IIIc) is shifted to more negative potentials due to the blocking of the active sites. In addition, when the potential scan is reversed, the stripping peaks appearing as the reversal of the small peak Ic' are more complex than those observed in Fig. 3a and b, suggesting a different mechanism of formation of a ZnCo alloy. Signal IIc appears as a small shoulder, and the stripping of a cobalt-rich deposit still occurs in the presence of this additive, and at more positive potentials the desorption of adsorbed hydrogen is detected as signal H.

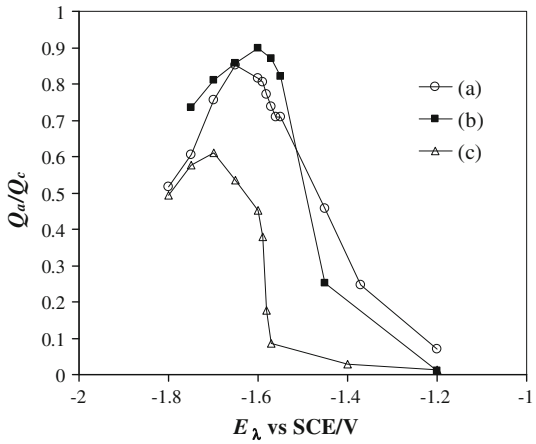

Fig. 4 Influence of organic aldehydes on the current efficiency (Qa/Qc) for ZnCo-alloy electrodeposition, plotted as a function of the E_λ. (**a**) S_2, (**b**) S_2 + 5 mM vanillin, (**c**) S_2 + 5 mM anisaldehyde

These results show that different stripping signals are obtained when different E_λ values are applied. Therefore, according to the stripping signals of the cyclic voltammetries, the addition of additives, especially *p*-anisaldehyde, modifies the electrochemical behavior and therefore also the deposit composition obtained at a particular potential. In addition, the behavior of the voltammograms recorded during ZnCo electrodeposition (Figs. 1, 2, 3) indicates that cobalt deposits at more positive potentials than zinc.

Figure 4 presents the ratio (Q_a/Q_c) between the charges passed in the anodic (Q_a) and cathodic (Q_c) peaks, which were calculated from the cyclic voltammograms for different switching potential values and may be interpreted as the current efficiency of the ZnCo-alloy electrodeposition process. The variation of the efficiency shows that a maximum is attained for E_λ around −1.60 to −1.70 V vs SCE. The decrease of the charge ratio at more negative potentials may be attributed to the effect of the HER, which is favored under such conditions. In addition, the effects of the additives modifies the electrodeposition efficiency (for $E_\lambda = -1.60$ V vs SCE) as shown by the increase of the charge ratio and hence efficiency with addition of vanillin but by a decrease of efficiency with the addition of anisaldehyde.

3.2 Characterization of the coatings

3.2.1 Composition of the deposits

Glow discharge spectroscopy (GDS) [40, 41] was used to investigate the elemental composition of deposits [5–7, 42–44]. Thin films of Zn and ZnCo deposits were obtained by electrodeposition on steel electrodes under steady conditions. The steel disk electrode was placed vertically to avoid the occlusion of the hydrogen bubbles formed during

HER and to promote natural convection. Deposits were obtained under both potentiostatic and galvanostatic conditions with similar results; subsequently potentiostatic deposition was used to produce specimens for study. Analysis of the deposit composition was performed to determine the cobalt, oxygen, carbon, and zinc contents in the resulting films.

Figure 5 presents the variation of the elemental weight percentages across the alloy coatings produced at −1.68 V. For ZnCo electrodeposits obtained from solution S_2 without additives (Fig. 5a), the cobalt content attained a maximum value around 2.5% when close to the steel substrate. Beyond this zone, the cobalt content decreased progressively until dropping off near the outer surface. This graph shows that codeposition was anomalous under these conditions, as the relative cobalt concentration in the solution was 3.48% w/w. A low level of oxygen was detected within the film, which increased near the outer surface. The profile of cobalt content within the deposit suggests that several steps take place during ZnCo electrodeposition, and indeed different mechanisms may prevail as the interface changes and the film grows. Different ZnCo alloy phases can be formed [33], such as γ2(91−92.8% Zn), γ1(87.4−88.6% Zn), γ(75.2−85.4% Zn), β(53−53.8% Zn), and the η-phase (%Co <3%). The cobalt level determined in the potentiostatically deposited ZnCo alloy films corresponds most closely to the hexagonal-close-packed (hcp) η-phase (%Co <3%). The stripping peaks of voltammograms depicted in Figs. 2 and 3 may correspond to variations of the relative amounts of zinc and cobalt in the η-ZnCo [33] alloy as well as some cobalt-rich phase formed at the beginning of the alloy deposition on the steel surface.

The addition of vanillin (Fig. 5b) presents deposit-composition behavior similar to that observed in the absence of additives. The cobalt level shows a maximum near the steel-alloy interface, becomes uniform, and then decreases near the outer surface of the deposit. The carbon content increases a bit near the alloy-steel interface, but in general terms it maintains the same order of magnitude. The presence of oxygen is also observed, and in this case its level appears to be increased by ten times; its presence is not related to the incorporation of the organic additives, as the carbon content is low, but the additive seems to introduce more oxygen from the electrolyte. The cause probably involves some intermediates generated during the reduction of vanillin.

Addition of anisaldehyde decreases the relative amount of cobalt in the deposit, which is uniform across the width of the thin ZnCo layer and stays close to 1.2%. In addition, the deposit thickness measured in Fig. 5c was lower than those obtained with the specimens for Fig. 5a and b. An enhancement of the HER was observed during the electrodeposition from electrolytes containing anisaldehyde. This phenomenon causes the decrease of both deposit thickness and process efficiency, in accordance with the smaller peaks IIc and IVa seen in Fig. 2. In general, the

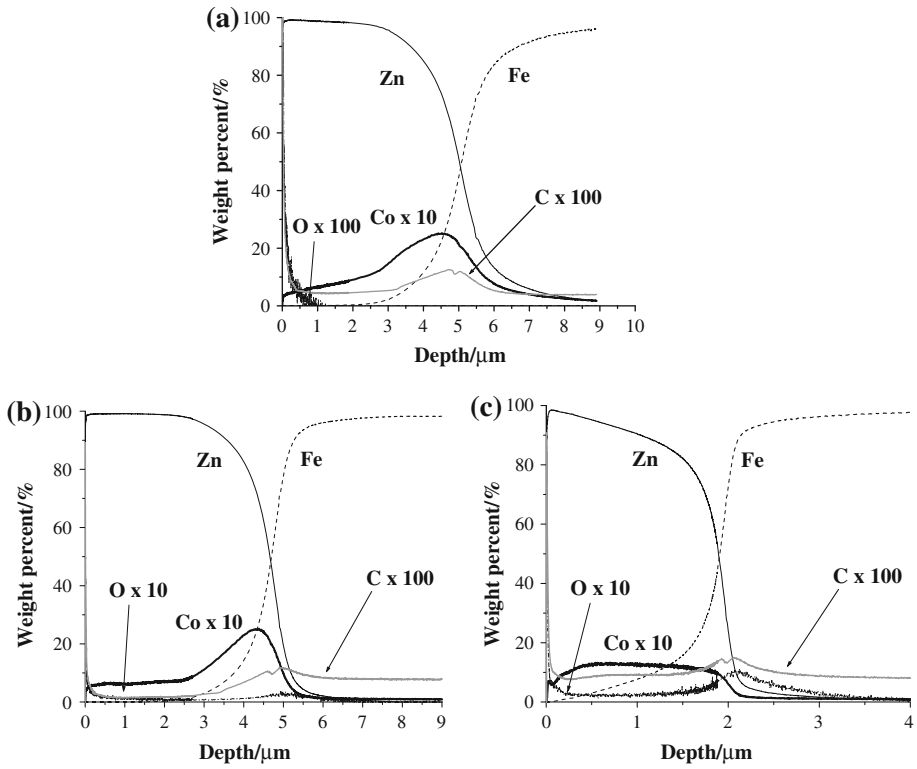

Fig. 5 Composition profiles with depth by GDS analysis for ZnCo deposits obtained from (**a**) solution S_2, (**b**) S_1 + 5 mM vanillin, (**c**) S_2 + 5 mM anisaldehyde. E_{appl} = −1.68 V, t = 180 s, S_2: 0.25 M $ZnCl_2$ + 4.0 M NaOH + 0.01 M $CoCl_2$ + 0.15 M NaL

relative level of cobalt in the deposits is a bit higher in the presence of anisaldehyde and seems to be rather constant.

Lehmberg et al. [42], El Hajjami et al. [43] and Mahieu et al. [44] also observed an increase of the alloying metal content close to the steel interface for acidic ZnNi [42], alkaline ZnNi [43], and acidic ZnCo [44] solutions. In acidic electrolytes, this observation was explained by an initial formation of Ni (or cobalt) deposit from the adsorption of insoluble $Ni(OH)_2$ resulting from the simultaneous reduction of hydrogen that increases the interfacial pH [42]. In alkaline conditions, such an interpretation does not explain the cobalt content profile along the cross section of the deposit. In alkaline baths for ZnNi [43], those authors proposed an initial reduction of nickel competitive with HER, suggesting that there is evidence of the formation of NiH_2 species in the interfacial steel/ZnNi layer. Figures 1, 2 and 3 show that some cobalt deposition takes place on steel before bulk zinc deposition occurs; such evidence may explain the increase of cobalt level near the steel surface at the early stages of electrodeposition (see Fig. 5). However, as the deposition of the alloy continues, the cobalt content decreases, leading to an anomalous deposit. Factors such as a difference in the exchange current values between zinc and cobalt [45] on the alloy surface and/or the Zn upd process [46–48] could explain the preferential electrodeposition of Zn, i.e., the anomalous deposition mechanism.

3.2.2 *Morphological study*

It is known that the addition of foreign substances to metal electrodeposition baths produces changes in the final morphology of the resulting coatings [38]. Different morphologies are obtained also when modifying the applied potential and/or current density, temperature and other factors [49–55]. Winand [50, 51] indicated that the shape of crystals is the result of a competition between parallel and perpendicular growth with respect to the substrate, the former requiring lower overpotentials than the latter. These changes are related to the electrodeposition mechanism, and therefore a specific morphology is obtained in a given situation [54].

Figure 6 shows the effect of the addition of vanillin and anisaldehyde on the morphology of ZnCo electrodeposits. Figure 6a shows that those deposits formed from solution S_0 (pure Zn plating bath) present typical hexagonal Zn crystals forming platelets with a boulder morphology formed under mixed activation and diffusion control [54].

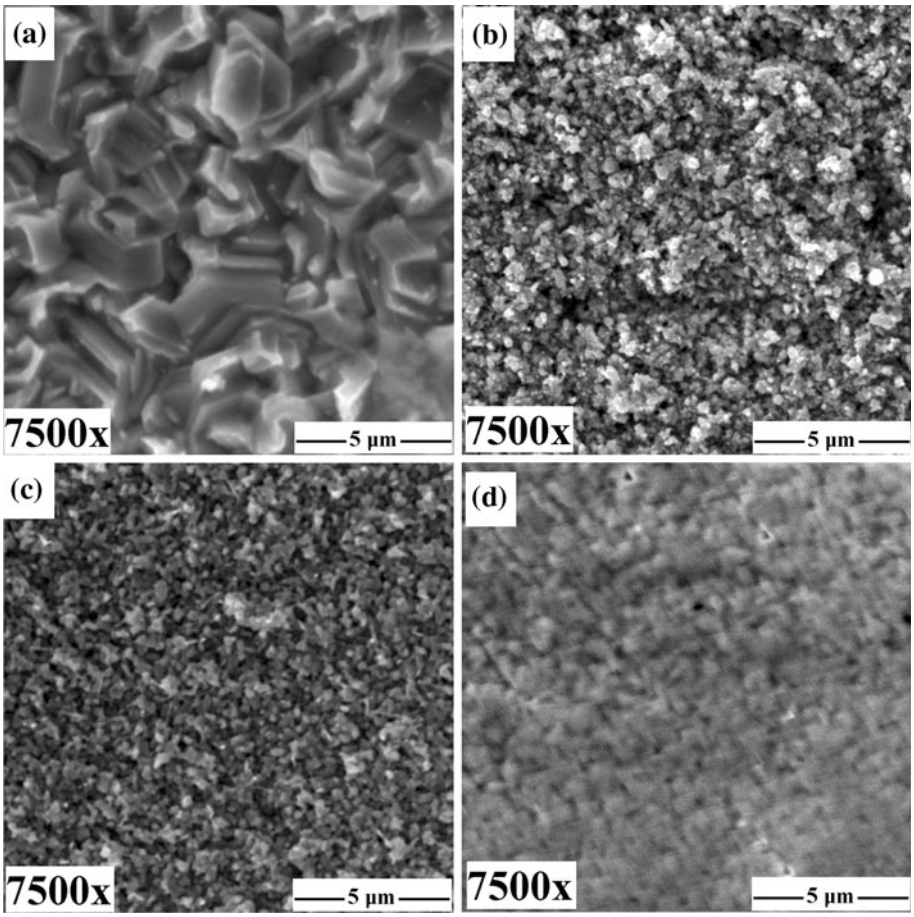

Fig. 6 SEM images of ZnCo deposits obtained from different electrolytes: (**a**) solution S_0, (**b**) solution S_2, (**c**) S_2 + 5 mM vanillin, (**d**) S_2 + 5 mM anisaldehyde. $E_{appl} = -1.68$ V vs SCE, t = 180 s. S_2: 0.25 M $ZnCl_2$ + 4 M NaOH + 0.15 M NaL + 0.01 M $CoCl_2$

When ZnCo deposits were formed from solution S_2 in the absence of additives (Fig. 6b), the SEM image shows a porous structure for ZnCo obtained at −1.68 V. This morphology differs from pure Zn deposits being characterized by hexagonal crystals under similar deposition conditions [7]. The presence of cobalt-gluconate complexes affects the mechanism of crystal growth, thus leading to smaller grains but porous deposits. This is possible if we consider that $CoL_3(OH)_2^{3-}$ and $CoL(OH)_2^-$ species are the primary forms of Co in the alkaline-gluconate solution, and decomplexation reaction would be the rate determining step during Co(II) discharge. The diminution of the crystal sizes can often be explained in terms of the inhibition effect of the additive [50, 51], due to its possible adsorption on the surface of the electrode [38]. Vermilyea indicated that crystal-size refinement is associated with surface adsorption by species that block the lateral propagation of lattice steps present during crystal growth [55]. In this case, inhibition of the electrochemical deposition signal is not observed, then, cobalt species would affect the crystal growth but do not produce smooth leveled deposits, thus forming porous coatings.

The addition of vanillin modifies slightly the morphological characteristics of the ZnCo deposits (Fig. 6c). A porous morphology is obtained when adding vanillin in the alkaline-gluconate electrolyte, but a more leveled surface is obtained in such conditions. The cyclic voltammogram of Fig. 2 shows that the experimental applied potential used to produce these specimens is in the range corresponding to the catalytic effect: the observed morphological changes are then imposed by the presence of Co that decreases the grain size of ZnCo deposits without and with vanillin, but the presence of the organic additive helps to decrease the deposit roughness. Such a result is in agreement with the voltammetric curves of Figs. 2 and 3b, which reveal a similar electrochemical response in the cathodic scan with and without vanillin.

The addition of anisaldehyde leads to a bright coating whose micrograph shows a smooth deposit with smaller grain size (Fig. 6d). The presence of holes over the deposit indicates that the HER occurs during the codeposition of the ZnCo alloy. A previous study devoted to the effects of mixtures of polyvinyl alcohol with aldehydes (anisaldehyde, piperonal and veratraldehyde) has shown that fine-grained deposits are obtained with those additives [11]. Mirkova et al. [18] also observed that the addition of anisaldehyde to a polymeric additive provides fine-grained Zn deposits. These effects are consistent with those observed in the voltammetric results depicted by Figs. 1 and 3c, which indicate a change in the reduction mechanisms with two steps occur during the cathodic scan.

The mechanism of action of additives is still a matter of study, and many efforts have been made to understand the influence of organic molecules during metal electrodeposition [56, 57]. The addition of such molecules often diminishes the grain size [38]. Kardos and Foulke [58] proposed three possible mechanisms to obtain bright deposits: leveling controlled by diffusion, grain refining, and randomization of crystal growth. Hoar [59] argued that selective or random nucleation mechanisms take place during electrodeposition. Selective nucleation is favored at low oversaturation on energetically favored sites such as kinks, steps, and dislocations among others. On the other hand, random deposition occurs on the entire surface; it is often promoted by the presence of additives that are adsorbed on the active sites. Oniciu and Muresan [38] indicated that the leveling mechanism is related to the increase of the overpotential registered during metal electrodeposition, which is in agreement with the observations presented in this study for anisaldehyde. According to Oniciu and Muresan [38], the main cause of the increase of the overpotential of metal reduction is due to the electrosorption of additives on the electrode surface, which diffuses and adsorbs preferentially on elevations rather than recesses, and therefore, leveled deposits are obtained as a consequence. The brightening mechanism would include a randomization of the nucleation sites, i.e., nucleation is favored ahead of crystal growth. Thus, the presence of Co ions favors nucleation, but irregular, non-leveled deposits are obtained; the overpotentials in this case do not shift appreciably. In the presence of anisaldehyde, the overpotential is increased, and the deposit morphology observed is regular and leveled. The bright deposit surface is explained in terms of more frequent nucleation.

3.2.3 *Crystallographic characterization*

Previous studies have shown the important role of the experimental conditions in changing the texture or crystallographic orientations of electrodeposits [60]. Additives also modify the preferential orientation of the crystal lattice [61] as shown for Zn [62, 63] and ZnCo [5, 7, 8, 64]. Previous studies showed that the preferential orientation of Zn changes with the applied potential during pulse plating conditions [65]. At low overpotentials, the formation of the basal (002) plane (which has the lowest energy of formation) is favored. Low-index pyramidal (104) and (103) planes appear when the potential of Zn deposition increases [65]. At higher potential, high-index pyramidal (112) and (101) planes are formed. Prismatic (110) and (100) orientations are expected at the highest applied potentials during Zn deposition. In addition, the angle of planes formed respect to the basal (002) plane increases as the overpotential becomes greater [64]. The authors observed that, under the experimental conditions of the reported study, the results showed a trend that was explained in terms of

atomic packing density: low overpotentials favor the formation of crystallographic planes having high-atomic packing density, and textures with low atomic packing density require high overpotentials [65].

Figure 7 shows the effects of the organic additives studied here on the crystallographic patterns of the same ZnCo coatings prepared under potentiostatic conditions. Curve a shows the typical diffraction pattern obtained for Zn deposits (JPDF 04-0831) [7], with a dominant peak associated with the crystallographic basal orientation plane (002) followed by the less intense peaks of pyramidal orientation planes (101), (103), (102) and (112).

On the other hand, the crystallographic pattern of the ZnCo alloy deposit presents some differences (Fig. 7, line b). The peak of plane (002) is suppressed, indicating that the preferential orientation changes. Various small peaks (labeled i) appear around $2\theta = 38°$, whereas the dominant peak is that associated with plane (101). The observed preferential peak (i) in Fig. 7, line b, could be attributed to the shift of the peak of plane (100), and related to the distortion of the crystal lattice. On the other hand, peaks seen in pure Zn deposits remain but with lower intensity, indicating the presence of a zinc-rich (η-phase) ZnCo alloy [65] since the diffraction pattern of the ZnCo solid solution η-phase is very similar to the pure-Zn diffraction pattern [66]. These results are confirmed by the composition analysis presented in Fig. 5, where anomalous Zn-rich ZnCo deposits were obtained under these experimental conditions.

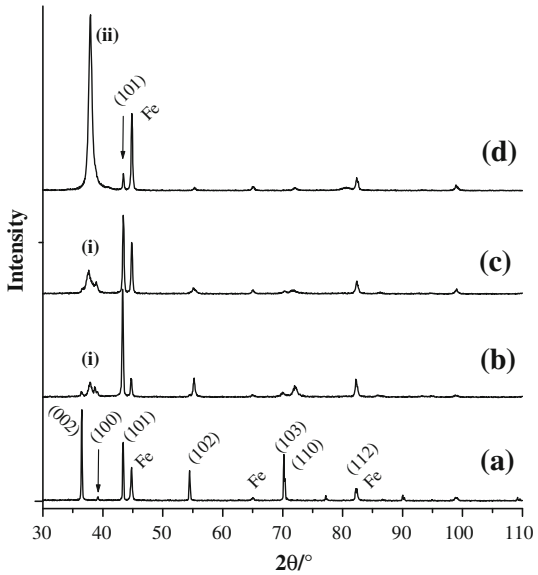

Fig. 7 Effects of the additives on the X-ray diffraction patterns of the Zn and ZnCo deposits, obtained under potentiostatic conditions. (**a**) solution S_0, (**b**) S_2, (**c**) S_2 + 5 mM vanillin, (**d**) S_2 + 5 mM anisaldehyde. $E_{appl} = -1.68$ V vs SCE, t = 180 s

In the presence of vanillin, (Fig. 7, line c), it is observed a similar diffraction pattern compared to the ZnCo deposit without organic additive (Solution S_2). The peak of plane (102) is diminished slightly compared to that observed for the no-additive ZnCo deposit. It is noted that the morphology does not change. The presence of anisaldehyde (Fig. 7, line d) affects the peak associated with planes (002), (100), (103), (102), (110), and (112), showing a small peak for plane (101). On the other hand, a dominant peak appears at $2\theta = 37.95°$, (labeled ii) characterized by a wider half-peak than those observed without additives and in the presence of vanillin. This observation denotes a preferential plane growth due to changes in the crystal habit of η-ZnCo related to the presence of the additive. A similar result has been obtained for ZnCo electrodeposition in the presence of *N*-benzyl-3-carboxylpyridinium [7, 8], where a dominant crystallographic peak appeared at $2\theta = 37.52°$ followed by a smaller peak of plane (101). Accordingly, anisaldehyde also affects the crystal lattice growth, and therefore a preferential orientation of the planes was changed, and bright deposits were obtained. Anisaldehyde and/or *N*-benzyl-3-carboxylpyridinium additives both exert strong effects during ZnCo electrodeposition, and the orientations of the deposits are identified as retaining the hexagonal structure. It is known that the peak width of a specific phase of a given material is inversely related to the mean crystallite size of that material. In this case, the wider signal appearing in the presence of anisaldehyde could be attributed to smaller grains.

The grain size (D) of the zinc deposited in the absence and in the presence of additives is calculated using the Debye–Scherrer formula $D = 0.9\lambda/\beta \cos\theta$ where λ is the wavelength of the x-ray used, β is the is the full width at half maximum, and θ is the diffraction angle [67]. The crystallite size (D) is estimated to be 320 nm for (101) plane of cubic Zn of solution S_0 and 80 nm for η-ZnCo obtained from solution S_2. In the presence of additives, the calculated grain size diminishes even more: in the presence of vanillin and anisaldehyde, the grain sizes are 76 and 60 nm, respectively. The broad peak located at $2\theta = 37.52°$ (obtained from solution S_2 in the presence of anisaldehyde) gives a grain size of 16.64 nm. These results show the tendency observed in Fig. 6 where the grain sizes diminish in the presence of cobalt ions and of additives. The sizes of the superficial crystals observed by SEM seem to be greater than those calculated from the Debye–Scherrer equation, possibly due to the formation of smaller crystals into the deposits.

These crystallographic results agree with the electrochemical study and the compositional analysis. It is confirmed that the η-ZnCo phase is formed, especially when *p*-anisaldehyde is added to the solution. Therefore, signal IIIa in Fig. 3c seems to correspond to this Zn-rich phase.

The stripping peak IVa in Fig. 3c is related to a cobalt-rich deposit and corresponds to reduction signal IIc in Fig. 2; i.e., the cobalt-rich deposit is formed before bulk Zn-rich ZnCo deposition occurs in peak Ic. However, anomalous deposits are obtained without and with the additives, and the GDS analysis shows a diminution of cobalt content as potentiostatic deposition proceeds. The addition of additives influences the electrochemical, morphological, and crystallographic characteristics. Brightening additive anisaldehyde provokes the most significant changes: an increase in the reduction overpotential for massive Zn reduction was obtained along with a fine-grained structure and an oriented texture. Further studies are needed to understand the underlying mechanisms of ZnCo electrodeposition, how the addition of aromatic aldehydes modifies them, as well as how the plating parameters determine the morphological, chemical, and crystallographic characteristics of the deposits.

4 Conclusions

ZnCo deposits were obtained from alkaline-gluconate electrolytes without and with aromatic aldehydes (vanillin and anisaldehyde). Although these molecules contain similar functional groups, their effects on the electrochemical, morphologic, and crystallographic characteristics of the deposits differ significantly. Vanillin does not bring appreciable changes to the electrochemical response for massive ZnCo deposition under the conditions of this study, but it seems to catalyze the HER at more negative potentials. Anisaldehyde suppresses partially the metal discharge and increases the overpotential for ZnCo deposition: it appears that a primary reduction occurs on free active surface sites while a second reduction process takes place on previously blocked sites on the steel surface. Stripping peaks are modified by the formation of different ZnCo phases. During potential scanning a cobalt-rich deposit is obtained on steel at potentials less negative than massive zinc-rich ZnCo deposition both in the absence and in the presence of the additives, in accordance with the nobler nature of cobalt. This preceding signal of cobalt-rich deposition is affected by the presence of the additives indicating an inhibition effect by the organic compounds. At more cathodic potentials zinc reduction occurs, and deposition becomes anomalous.

The analysis of the elemental composition in films formed potentiostatically demonstrates that the resulting deposits are generally anomalous, the Co:Zn ratio in the deposit being lower than that in solution. A slight elevation in the cobalt content near the steel surface indicates preferential partial deposition of cobalt in the early stages of the process, but it is inhibited as the deposition proceeds. Pure Zn formed boulder-like deposits, but in the presence of Co, the grain size was diminished, indicating a strong effect on crystal growth and morphology by blocking of lateral motion of the crystal lattice. The presence of vanillin with the alloy also presents porous morphology with small crystals, which shows that the main effect is due to the presence of Co. The morphology of the ZnCo deposits changes from porous to granular and compact fine-grained deposits in the presence of anisaldehyde. Crystallographic peaks were also modified. The addition of Co had significant influence on the (002) plane. ZnCo deposits obtained in the presence of vanillin presented a similar pattern and texture. Anisaldehyde changed the orientation of the ZnCo deposits and produced a highly oriented texture. The formation of the zinc rich η-ZnCo alloy was confirmed in all the cases. The observed structural effects are consistent with the measured electrochemical properties of these plating baths.

Acknowledgments The authors thank CONACYT (Consejo Nacional de Ciencia y Tecnología), México, (Project. 31411 and PCP) for financial assistance. J.L. Ortiz-Aparicio is also grateful for CONACYT scholarships. The authors also thank M. Vega-González and M. Aguilar-Franco of the Instituto de Física, Universidad Nacional Autónoma de México, for the experimental help and discussion of the X-rays diffraction patterns.

References

1. Geduld H (1988) Zinc plating. ASM International, Metals Park
2. Winand R (2000) In: Schlessinger M, Paunovic M (eds) Modern electroplating, Electrochemical society series. Wiley, New York
3. Crotty DE (1991) Met Finish 89:58
4. Brenner A (1963) Electrodeposition of alloys, vol 1. Academic Press, New York
5. Trejo G, Ortega R, Meas Y et al (2003) J Appl Electrochem 33:373
6. Ortiz-Aparicio JL, Meas Y, Trejo G et al (2007) Electrochim Acta 52:4742
7. Ortiz-Aparicio JL, Meas Y, Trejo G et al (2008) J Electrochem Soc 155:D167
8. Ortiz-Aparicio JL, Meas Y, Trejo G et al (2009) J Electrochem Soc 156:K205
9. Pereira MS, Barbosa LL, Souza CAC et al (2006) J Appl Electrochem 36:727
10. Ramesh Bapu GNK, Devaraj G, Ayyapparaj J (1998) J Solid State Electrochem 3:48
11. Shanmugasigamani, Pashpavanam M (2006) J Appl Electrochem 36:315
12. Rethinam AJ, Ramesh Bapu GNK, Muralidharan VS (2003) Trans Inst Met Finish 81:136
13. Zhu J, Zhou Y, Gao C (1998) J Power Sources 72:231
14. Narasimhamurthy V, Sheshadri BS (1998) Met Finish 96(4):24
15. Narasimhamurthy V, Sheshadri BS (1999) Trans Inst Met Finish 77:29
16. Darken J (1979) Trans Inst Met Finish 57:145
17. James BS, McWhinnie WR (1980) Trans Inst Met Finish 58:72
18. Mirkova L, Monev M, Krastev I, Rashkov S (1995) Trans Inst Met Finish 73:107

19. Monev M, Mirkova L, Krastev I et al (1998) J Appl Electrochem 28:1107
20. Roev VG, Kaidrikov RA, Khakimullin AB (2001) Russ J Electrochem 37:756
21. Loshkaryov YM, Vlinov VM, Gnedenkov LY et al (1989) Bull Electrochem 5:254
22. Titova VN, Javich AA, Petrova NV et al (2000) Bull Electrochem 16:425
23. Titova VN, Kazakov VA, Yavich AA et al (1996) Russ J Electrochem 32:562
24. Kim SJ, Kim HT, Park SM (2004) J Electrochem Soc 151:C850
25. Huang F, Pan SX, Liang Y (1992) Plat Surf Finish 79(1):64
26. Jow JJ, Chou TC (1987) Electrochim Acta 32:311
27. Kavitha B, Santhosh P, Renukadevi M et al (2006) Surf Coat Technol 201:3438
28. Cain KJ, Melendres CA, Maroni VA (1987) J Electrochem Soc 134:519
29. Zhang Y, Muhammed M (2001) Hydrometallurgy 60:215
30. Wijenberg JHOJ, Stevels JT, de Wit JHW (1998) Electrochim Acta 43:649
31. Maleeva EA, Pedan KS, Ponjomarev II (1996) Russ J Electrochem 32:1380
32. Gabe DR (1997) J Appl Electrochem 27:908
33. Panagopoulos CN, Georgarakis KG, Petroutzakou S (2005) J Mater Process Tech 160:234
34. Swathirajan S (1986) J Electrochem Soc 133:671
35. Gómez E, Vallés E (1995) J Electroanal Chem 397:177
36. Gómez E, Vallés E (1995) J Electroanal Chem 421:157
37. Gómez E, Alcobe X, Vallés E (2001) J Electroanal Chem 505:54
38. Oniciu L, Muresan L (1991) J Appl Electrochem 21:565
39. Kaneko N, Shinohara N, Nezu H (1993) Electrochim Acta 38:1351
40. Angeli J, Bengtson A, Bogaerts A et al (2003) J Anal At Spectrom 18:670
41. Pisonero J, Fernández B, Pereiro R et al (2006) Trends Anal Chem 25:11
42. Lehmberg CE, Lewis DB, Marshall GW (2005) Surf Coat Technol 192:269
43. El Hajjami A, Gigandet MP, De Petris-Wery M et al (2007) Appl Surf Sci 254:480
44. Mahieu J, De Wit K, De Boeck A et al (1999) J Mater Eng Perfom 8:561
45. Mathias MF, Chapman TW (1987) J Electrochem Soc 134:1408
46. Nicol MJ, Philip HI (1976) J Electroanal Chem 70:233
47. Ohtsuka T, Komory A (1998) Electrochim Acta 43:3269
48. Swathirajan S (1987) J Electroanal Chem 221:211
49. Bockris JOM, Zagy N, Drazic D (1973) J Electrochem Soc 120:30
50. Winand R (1992) Hydrometallurgy 29:567
51. Winand R (1994) Electrochim Acta 39:1091
52. Mansfeld F, Gilman S (1970) J Electrochem Soc 117:588
53. Sonneveld PJ, Visscher W, Barendrecht E (1992) Electrochim Acta 37:1199
54. Wang RY, Kirk DW, Zhang GX (2006) J Electrochem Soc 153:C357
55. Vermilyea DA (1959) J Electrochem Soc 106:66
56. Damaskin BB, Petrii OA, Batrakov VV (1971) Adsorption of organic compounds on electrodes. Plenum Press, New York
57. Dini JW (1993) Electrodeposition. Noyes Publications, Park Ridge
58. Kardos O, Foulke DG (1962) In: Tobias CW (eds) Advances in electrochemistry and electrochemical engineering, vol 2. Interscience Publisher, New York
59. Hoar TP (1953) Trans Inst Met Finish 29:7566
60. Pangarov NA (1965) J Electroanal Chem 9:70
61. Denise F, Leidheiser H (1953) J Electrochem Soc 100:490
62. Sekar R, Jayakrishnan S (2006) J Appl Electrochem 36:591
63. Mouanga M, Ricq L, Douglade J et al (2007) J Appl Electrochem 37:283
64. Mouanga M, Ricq L, Berçot P (2008) Surf Coat Technol 202:1645
65. Youssef KM, Koch CC, Fedkiw PS (2008) Electrochim Acta 54:677
66. Bajat JB, Mišković-Stankovic VB, Maksimović MD et al (2002) Electrochim Acta 47:4101
67. Guinier André (1994) X-ray diffraction in crystals, imperfect crystals, and amorphous bodies. Dover Publications, Toronto